ELSEVIER

Chemical Engineering Journal 144 (2008) 153–166

Chemical Engineering Journal

www.elsevier.com/locate/cej

Studies on the understanding mechanism of air core and vortex formation in a hydrocyclone

R. Gupta [a], M.D. Kaulaskar [a], V. Kumar [a], R. Sripriya [b], B.C. Meikap [a,*], S. Chakraborty [a]

[a] *Department of Chemical Engineering, Indian Institute of Technology, Kharagpur 721 302, India*
[b] *Tata Steel, R&D Division, Jamshedpur, Jharkhand 831007, India*

Received 8 November 2007; received in revised form 25 December 2007; accepted 4 January 2008

Abstract

A hydrocyclone is cyclone that uses water as a bulk fluid. The advantages like low cost, no moving parts, little maintenance cost and high capacity make it attractive for industrial use. During the operation, due to the low pressure at cyclone axis, a back-flow of gas can occur which then forms a gas-core. This gas-core affects the separation efficiency. This gas-core was eliminated by inserting a solid rod. Experiments were made in a newly constructed hydrocyclone for different inlet flow rate in presence as well as in absence of gas-core to qualify the pressure drop characteristics of the hydrocyclone. Effect of gas-core on the pressure between different specific locations was studied. FLUENT as a CFD-modelling tool was used for hydrodynamic study.

Keywords: Hydrocyclone; Air core; FLUENT; Hydrodynamics; CFD

1. Introduction

The cyclone is a simple device, which causes the centrifugal separation of materials in a fluid stream. Unlike the slow setting within a settling tank, the pump and cyclone separator system yields fast separation and utilizes less space. Separations occur quickly because one "g" of gravitation force is replaced by many "g"s of centrifugal force.

These materials may be particles of solid, bubbles of gas or immiscible liquids. In the case of two solids suspended in the feed liquid they may separate according to size, shape, or density. The cyclone utilizes the energy obtained from fluid pressure to create rotational fluid motion. This rotational motion causes the materials suspended in the fluid to separate from one another or from the fluid quickly due to the centrifugal force.

The rotation is produced by the tangential or involuted introduction of fluid into the vessel. A hydrocyclone is a cyclone separator that uses water as the bulk fluid. Hydrocyclones are becoming well established in industrial applications. Applications of hydrocyclones fall into several broad categories; clarification, thickening, classification, sorting, washing, liquid–liquid separation, liquid degassing and particle size measurement. They are frequently used as protection or pre-treatment devices to improve the performance or decrease the cost of down stream equipment. The target industries include mineral processing, mining, petrochemicals, oil production, wastewater and effluent treatment, food processing, pharmaceuticals, and other industries dealing with slurries.

The cyclone consists of a vertical cylinder with a conical bottom. Generally, typical hydrocyclones have a tangential feed inlet and two outlets; one for the concentrated solids (underflow) and one for the relatively clean liquid reporting out of the vortex finder tube (overflow). Hydrocyclones have no moving parts, and pumping the fluid tangentially into the stationary cono-cylindrical body produces the essential whirling motion. The cylindrical part is closed at the top by a cover, through which the liquid overflow pipe, known as the vortex finder, extends some distance into the cyclone body. It is necessary that the end of the vortex finder extend below the feed inlet to reduce premature exit of the overflow.

Located near the top cover is either a circular or rectangular feed opening where liquid enters the hydrocyclone through the tangential inlet. The underflow leaves through a hole in the apex of the cone. Both spirals rotate in the same direction.

The separation action of a hydrocyclone treating particulate slurry is a consequence of the swirling flow that produces a cen-

* Corresponding author. Tel.: +91 3222 283958; fax: +91 3222 282250.
E-mail address: bcmeikap@che.iitkgp.ernet.in (B.C. Meikap).

1385-8947/$ – see front matter © 2008 Elsevier B.V. All rights reserved.
doi:10.1016/j.cej.2008.01.010

trifugal force on the fluid and suspended particles. The feed slurry is injected tangentially into the hydrocyclone at high velocity to produce a large centrifugal force field. The feed moves down the wall rapidly and generates a helical vortex, which extends beyond the lower end of the vortex finder. This swirling flow is highly turbulent and three-dimensional. In the centrifugal field, the particles move relative to the fluid with respect to the balance of centrifugal and drag forces acting upon particles in the radial direction, such that classification occurs. The coarser or heavier particles move toward the wall and are swept downward to the apex of the cone. The fluid phase that carries the smaller or lighter particles approaches the apex and reverses in the axial direction spiraling upward and leaving the hydrocyclone through the vortex finder. Along the axis, an area of low pressure is created by the very high angular momentum. This may cause the formation of a rotating free liquid surface at the centre. If the hydrocyclone is opened to the atmosphere, air is inhaled through the apex and forms an air core. In that case, the pressure at the air–liquid interface is equivalent to atmosphere pressure (neglecting both the surface tension and viscous forces).

Bretney [1] got the first patent on hydrocyclones. Despite this, it took half a century before they were extensively used. Since 1950, a range of papers has been published concerning the operation of hydrocyclones and some mathematical models describing velocity profiles, the pressure drop and the separation efficiency (Kelsall [2]). An extensive survey of the literature reveals that fundamental and applied research on the design and performance of hydrocyclone has been continuing for the last five decades. Kelsall [2] performed first systematic and detailed experimental work. His measurements of radial, axial and azimuthal velocity profiles served as a basis of many subsequent investigations. Kelsall [2] reported the flow pattern and velocity profiles within a hydrocyclone. Bradley and Pulling [3] studied the flow pattern in the hydraulic cyclone and their interpretation in terms of performance by dye injections into the fluid flowing in the hydrocyclone and have added to detailed knowledge of flow patterns [2]. The results are described and the implications on the theoretical correlation of efficiency are discussed. Such a correlation can never be precise owing to uncertainties in the path followed by an individual particle.

The major contribution in this field has been from Lynch and Rao [4]. The use of empirical equation is limited by the fact that the constants and coefficients of the equations need to be evaluated for each and every situation. Chu et al. [5] worked on numerical simulation of turbulence and structure of turbulence in hydrocyclone.

Very often, compartment models were used to describe flow characteristics in different regions in a hydrocyclone (inlet duct, boundary layer flow near to the wall, swirl in the centre, regions of the underflow and overflow) by semi-empirical or empirical approximate equations based on experiments. Also, numerical calculations using computational fluid dynamics (CFD) were realised. But often, the description of turbulence effects was simplified using the original or a modified form of the k–ε turbulence model or the Prandtl mixing length relation (Hsieh and Rajamani [6]). No work based on CFD was published which considers the unsteady behaviour of the flow field. For a prediction of a gas-core, only empirical relations are available (Steffens et al. [7]. The influence of the solid phase was not considered or the particle motion was described in a simple manner using an algebraic slip model (Dyakowski and Williams [8] and Steffens et al. [7]). Regarding higher solid phase concentrations, there exist some models to calculate the resulting boundary layer (Laverack [9]). The solutions of the resulting models were usually calculated using the authors' own programs. Dwari et al. [10] reported performance characteristics for particles of sand FCC and fly ash in a novel hydrocyclone. Ovalle and Concha [11] investigated the role of wave propagation in hydrocyclone operations II: wave propagation in the air–water interface of a conical hydrocyclone.

2. Flow characteristics in hydrocyclones

The flow behaviour in hydrocyclone is quite complex. This complexity of flow processes has led designers to rely on empirical equations for predicting the equipment performance. These empirical relationships are derived from an analysis of experimental data and include the effect of operational and geometric variables. Different sets of experimental data lead to different equations for the same basic parameters. Empirical models correlate classification parameters with device dimensions and slurry properties. However, these models suffer from the inherent deficiency as any other empirical models—the model can only be used within the extremes of the experimental data from which the model parameters were determined. In view of this shortcoming, mathematical models based on fluid mechanics are highly desirable. Computational fluid dynamics is a versatile mean to predict velocity profiles under a wide range of design and operating conditions. The numerical treatment of the Navier–Stokes equations is the backbone of any CFD technique gradually crept into the analysis of the hydrocyclone in the early 1980s. This resulted from the rapid improvement in computers and a better understanding of the numerical treatment of turbulence.

In the region near the central axis the vortex conservation was applied with inviscid and rotational flow assumptions, which yields axial and radial components. In the region along the wall the boundary layer approach was used to derive velocities. Using the simple Prandtl mixing length model and the axisymmetry assumptions, the authors reported the velocity predictions in a 200-mm hydrocyclone. Later, Hsieh and Rajamani numerically solved the turbulent momentum equations to obtain the velocities and compared them with the Laser Doppler Velocimetry measurements in a 75-mm hydrocyclone [6]. This work shows that, by a simple balance of forces on a particle present in the flow field, the trajectory of the particle can be traced inside the hydrocyclone, from which the entire size-classification efficiency can be computed. All of these modelling works have been confined to hydrocyclones processing slurries in the 5–10% solids range, and have mostly been restricted to axisymmetric geometries (Davidson [12]).

The practical constraints in carrying out 3D simulations have been the allocable memory and the total amount of CPU time that may be spent on the simulation. Most of the studies have

aimed to simulate only the flow of water in a hydrocyclone; very few attempts have been made to predict the flow of solids in the separator.

In the recent years, He et al. [13] did the numerical simulation of a hydrocyclone and described using the k–ε model that was corrected with a single empirical coefficient dependent on the Richardson number for the impact of the curved streamlines. Dai et al. [14] present numerical results for a hydrocyclone based on the k–ε turbulence model whose model parameters were fitted to experimental data. Results concerning pressure drop or separation behaviour are not given. To determine the separation characteristics, some analytical models were developed. Rietima [15] presented a model considering the mean residence time of a particle in the hydrocyclone. In the mineral processing field, air core dimension is a critical variable, since a large air core diameter leads to a condition known as roping. The primary computational approach reported in the literature (Dyakowski and Williams [8]) is axisymmetric approach, which reduced the computational domain to two coordinates, the radial and azimuthal axes.

The axisymmetry assumption greatly reduced the computational demand for the numerical solution. These approaches used Prandtl mixing length model or k–ε model or a variant of these models for turbulence closure. While these models were successful in their particular objectives, a full three-dimensional model is well suited for the single inlet which creates asymmetry. Furthermore, the development of the air core can only be studied with three-dimensional CFD.

The content of recent work comprises the design of special hydrocyclones for preventing the formation of a gas-core and some investigations for the explanation of the so-called "fish-hook effect", which characterizes the growing separation efficiency with smaller particle sizes (Frachon and Cilliers [16]).

This survey of literature shows that there is a range of work concerning the operation behaviour of hydrocyclones and some particular phenomena. But up to now, there is no work dealing with a comprehensive numerical model for calculating hydrocyclones on the basis of computational fluid dynamics which does not depend on special experimental conditions or particular cyclone geometry. Especially, the prediction of air core and vortex formation provides some difficulties and is almost not considered in the recent papers. For this reason, the progress in performing comprehensive numerical studies for hydrocyclones using computational fluid dynamics is described in the present work.

3. Separation efficiency

The term efficiency used here is a measure of the ability of the separator to recover solids in the underflow. Solids removal from the underflow is needed because a large majority of the fluid will continue through the overflow and through the rest of the process.

This simple description can result in perfect efficiency by directing all the feed materials into the underflow, recovering 100% of the feed solids in the underflow and 100% fluid out the overflow. Therefore, if the objective is to remove solids from aqueous slurry, the efficiency is summarized in the equation:

$$E = \frac{S_u}{S_i} - \frac{L_u}{L_i} \tag{1}$$

where E is the efficiency of separation of solids from feed to underflow, S is the amount of the solids present, L is the amount of liquids present, and the subscripts i and u refer to the inlet and underflow streams, respectively. If the objective of the cyclone is to separate two solids, however, one is not concerned with the distribution of the liquids and the separation efficiency can be considered as:

$$E = \frac{(\%\text{ of lights recovered in overflow} + \%\text{ of heavies recovered in underflow})}{2}$$

4. Air core and vortex formation

4.1. Formation of vortex

The vortex is formed physically in a hydrocyclone due to the swirling motion of the tangentially inlet liquid velocity and resulted in low pressure regime within the cyclone. Thus an aircore is formed. The air comes through the underflow of the hydrocyclone from atmosphere.

- In operation, pressurized slurry is fed to the hydrocyclones and the centrifugal force generated causes the heavier suspended solids to move toward the wall while the radial velocity forces the liquid and lighter gravity solids to move inward toward the centre axis.
- The flow pattern in a cyclone separator is a spiral within a spiral.
- Upon the tangential entry the fluid travels in a downward flow along the outside of the cyclone body. This plus the rotational motion creates the outer spiral.
- Primary and secondary vortex develops. The primary vortex carries the solids to the apex.
- The apex orifice permits the heavier solids and a small amount of the liquid to be discharged.
- Air is drawn through the apex and a secondary developing vortex carries the cleaned primary liquid and light gravity solids out through the vortex finder tube.
- An increase in inward migration occurs, closer to the cone apex and the fluid in this migratory stream reverses its vertical direction and flows upwards, to the overflow outlet.
- The spirals rotate in the same circular direction.

4.2. Formation of air core

- Due to the low pressure at the cyclone axis, a back-flow of gas can occur which then forms a gas-core.
- Experimental work has shown that the tangential velocity increases sharply with radius in the central core region under the vortex finder and that thereafter it decreases with radius,Kelsall [2].

- In the event of an air core forming it is necessary to account for the shape of the air core to correctly predict the flow split between the under and overflow.
- The low-pressure air core shape and size is a function of the swirling velocity field and the localized slurry density.
- The air core shape formed by the back-flow of air is strongly coupled to slurry concentration, and the predicted swirl.

5. Modelling of hydrocyclones

(a) Particle separation prediction
- *Slip velocities*: velocity of particles with respect to velocity of fluid.

(b) Dynamic force balance on particle
- *Radial direction*: centrifugal and drag force.
- *Axial direction*: gravitational force, buoyancy force and axial drag force.
- *Tangential direction*: no significant forces, considered to move along fluid.

In hydrocyclone flow fields the time for a particle to reach its terminal settling velocity is usually very short. The usual assumption made is that the particle moves at its settling velocity U_s, which is determined by a balance between the drag force F_d and the combined gravitational and centrifugal forces acting on the particle. The drag force is expressed as:

$$F_d = \frac{1}{2}\rho_L C_d A U_s^2 \tag{2}$$

While the combined gravitational and centrifugal forces are expressed component-wise as follows:

$$\begin{aligned} &\text{axial component}: \quad F_x = (\rho_p - \rho_l)Vg \\ &\text{radial component}: \quad F_r = \left(\rho_p \frac{\omega_p^2}{r} - \rho_l \frac{\omega_l^2}{r}\right) V \\ &\text{circumferential component}: \quad F_g = -\left(\rho_p \frac{v_p \omega_p}{r} - \rho_l \frac{v_l \omega_l}{r}\right) V \end{aligned} \tag{3}$$

In the above expressions, V is the volume of the particle and g is the gravitational acceleration.

Balancing the drag force with the external forces acting on the particle gives

$$\frac{1}{2}\rho_l C_D A U_S^2 = \sqrt{F_x^2 + F_y^2 + F_g^2} \tag{4}$$

Define

$$a = \sqrt{\left(1 - \frac{\rho_l}{\rho_p}\right)^2 g^2 + \left(\frac{\omega_p^2}{r} - \frac{\rho_l}{\rho_p}\frac{\omega_l^2}{r}\right)^2 + \left(\frac{v_p \omega_p}{r} - \frac{\rho_l}{\rho_p}\frac{v_l \omega_l}{r}\right)^2} \tag{5}$$

Then the settling velocity U_s can be written, for the case of spherical particles, as

$$U_S = \sqrt{\frac{4}{3}\frac{ad}{C_D}\frac{\rho_p}{\rho_l}} \tag{6}$$

First, the relative velocity or the slip velocity between the fluid and the particle is calculated. Then the particle Reynolds number is computed as

$$Re = \frac{\rho_l U_S d}{\mu} \tag{7}$$

A drag force on the particle is then calculated using this particle Reynolds number, and the following drag law expression taken from Clift et al. [17]

$$C_D = \frac{24}{Re}(1 + 0.15 Re^{0.687}) + \frac{0.42}{1 + 4.25 \times 10^4 Re^{-1.16}} \tag{8}$$

In each of the simulations, 200 particles having a certain diameter are randomly located at the inflow patch and their trajectories are traced until they exit the hydrocyclone either through the overflow or underflow orifice. Then a different particle size is assigned and repeated for a range of particle sizes. The results yield a particle separation efficiency curve.

5.1. Challenges in the modelling of hydrocyclones

- three-dimensional flow patterns,
- anisotropic turbulence,
- dispersed secondary phase,
- both high and low volume loadings,
- size distributions,
- particle to particle interactions,
- low-pressure central core,
- unstable flow structures may develop,
- numerical sensitivity and
- radial Pressure distribution on over and underflow boundaries.

5.2. Available models for modelling

Steady and unsteady particle tracking model

- Stochastic and particle cloud model for turbulent dispersion.
- Ability to include particle size distribution and include various forces and physics for particles (reaction), many UDF's and post processing capabilities.

Volume of fluid model (VOF model)

- Solves for the interface between g/l and l/l.
- Advanced front tracking to resolve interface.
- Effective for modelling the motion of large (much bigger than grid) bubbles.

LANGRAGIAN particle method

- Effective method for quantifying separation performance.
- Can be carried out as a coupled calculation or as a post processing exercise.
- Must use sufficient particles to ensure insensitive result.
- Release position/distribution at inlet will is reflected in the predicted separation performance.
- In a steady flow field particles, which may have only spent a fraction of a second in a swirling re-circulation, are held there indefinitely.

- Does not account for the volume occupied by dispersed material.
- No particle to particle interaction.

Algebraic slip mixture model

- Solves a single set of momentum equations for both continuous and dispersed phases (same velocity).
- Cannot simulate phases travelling in different directions.
- Dispersed phase must achieve terminal velocity quickly.
- Computationally cheap.
- Can be used to solve for air core but does not account for.
- Any interface effects, fluffy interface—cheap robust.
- Adequate when phases remain suspended.
- Struggles to resolve high dispersed phase concentrations at walls.

Eulerian–Eulerian granular model

- The most definitive multiphase model, which solves a separate set of momentum equations for each phase.
- Accounts for high volume loadings.
- Particle to particle interaction.
- Accurate predictions of air core development.
- High CPU cost when combined with RSM turbulence equations.

5.3. Continuity and momentum equations

For all flows, FLUENT solves conservation equations for mass and momentum. For flows involving heat transfer or compressibility, an additional equation for energy conservation is solved. For flows involving species mixing or reactions, a species conservation equation is solved or, if the non-premixed combustion model is used, conservation equations for the mixture fraction and its variance are solved. Additional transport equations are also solved when the flow is turbulent.

5.4. The mass conservation equation

The equation for conservation of mass, or continuity equation, can be written as follows:

$$\frac{\partial \rho}{\partial t} + \nabla(\rho \vec{v}) = S_{\mathrm{m}} \tag{9}$$

5.5. Momentum conservation equations

Conservation of momentum in an inertial (non-accelerating) reference frame is described by

$$\frac{\partial}{\partial t}(\rho \vec{v}) + \nabla(\rho \vec{v}\vec{v}) = -\nabla p + \nabla(\bar{\bar{\tau}}) + \rho \vec{g} + \vec{F} \tag{10}$$

where p is the static pressure, $\bar{\bar{\tau}}$ is the stress tensor (described below), and ρg and $\vec{F}$ are the gravitational body force and external body forces (e.g., that arise from interaction with the dispersed phase), respectively. $\vec{F}$ also contains other model-dependent source terms such as porous-media and user-defined sources.

The stress tensor $\bar{\bar{\tau}}$ is given by

$$\bar{\bar{\tau}} = \mu \left[(\nabla \vec{v} + \nabla \vec{v}^{\mathrm{T}}) - \frac{2}{3} \nabla \vec{v} I \right] \tag{11}$$

where μ is the molecular viscosity, I is the unit tensor, and the second term on the right hand side is the effect of volume dilation.

5.6. The standard k–ε model:

The standard k–ε model is semi-empirical models based on model transport equations for the turbulent kinetic energy (k) and its dissipation rate (ε), and are given by

$$\frac{\partial}{\partial t}(\rho k) + \frac{\partial}{\partial x_i}(\rho k u_i) = \frac{\partial}{\partial x_j}\left[\left(\mu + \frac{\mu_i}{\sigma_{\mathrm{k}}} \right) \frac{\partial k}{\partial x_j} \right] + G_{\mathrm{k}} - \rho \varepsilon \tag{12}$$

$$\frac{\partial}{\partial t}(\rho \varepsilon) + \frac{\partial}{\partial x_i}(\rho \varepsilon u_i) = \frac{\partial}{\partial x_j}\left[\left(\mu + \frac{\mu_i}{\sigma_{rm\varepsilon}} \right) \frac{\partial k}{\partial x_j} \right] + C_{1\mathrm{e}} \frac{\varepsilon}{k} G_{\varepsilon} - C_{2\mathrm{e}} \rho \frac{\boldsymbol{\varepsilon}^2}{k} \tag{13}$$

$$G_{\mathrm{k}} = -\rho \overline{u_i u_j} \frac{\partial uj}{\partial xi} \tag{14}$$

In these equations, G_{k} represents the generation of turbulent kinetic energy due to the mean velocity gradients; $C_{1\mathrm{e}}$, $C_{2\mathrm{e}}$ and $C_{3\mathrm{e}}$ are constants. σ_{k} and σ_{ε} are the turbulent Prandtl numbers for k and ε, respectively. The 'eddy" or turbulent viscosity can be computed by combining k and ε as follows

$$\mu_{\mathrm{t}} = \rho C_{\mu} \frac{\boldsymbol{k}^2}{\varepsilon} \tag{15}$$

where C_{μ} is a constant. The model constants $C_{1\mathrm{e}}$, $C_{2\mathrm{e}}$, C_1, σ_{k} and σ_{ε} were assumed to have the following default values:

$C_{1\mathrm{e}} = 1.44$, $C_{2\mathrm{e}} = 1.92$, $C_1 = 0.09$, $\boldsymbol{\sigma}_{\mathrm{k}} = 1.0$, $\boldsymbol{\sigma}_{\varepsilon} = 1.3$.

For a dilute fluid suspension, the incompressible Navier–Stokes equations supplemented by a suitable turbulence model are appropriate for modelling the flow in a hydrocyclone. The most popular turbulence model in use for engineering applications is the k–ε model where the scalar variables k and ε represent the kinetic energy of turbulence and its dissipation rate, respectively. These equations describe the conservation of mass, momentum, and turbulence kinetic energy and its dissipation rate.

$$\begin{aligned} &\rho \dot{u} \nabla \dot{u} - \nabla(\mu_{\mathrm{eff}} \nabla \dot{u}) = -\nabla p \\ &\nabla \dot{u} = 0 \end{aligned} \tag{16}$$

$$\nabla\left(\rho \vec{u} k - \frac{\mu_{\mathrm{t}}}{\sigma_{\mathrm{k}}} \nabla k \right) = G - \rho \varepsilon \tag{17}$$

$$\nabla\left(\rho \vec{u} \varepsilon - \frac{\mu_{\mathrm{t}}}{\sigma_{\varepsilon}} \nabla \varepsilon \right) = C_1 \frac{\varepsilon}{k} G - C_2 \rho \frac{\varepsilon^2}{k} \tag{18}$$

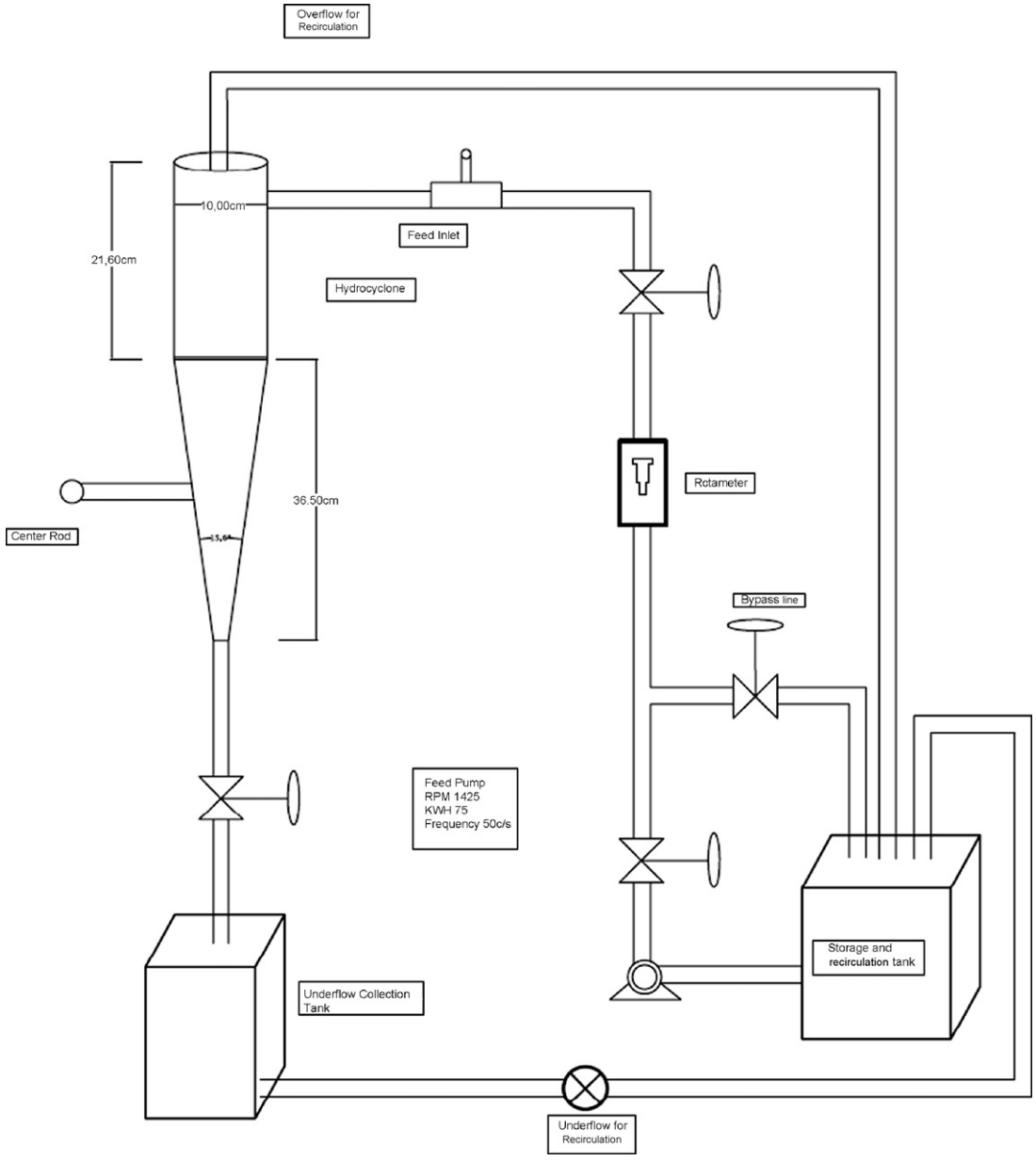

Fig. 1. Schematic of the experimental set up.

The computational method used is the finite volume discretization of the domain into computational cells where the conservation principle is enforced for each of the properties: mass, momentum, k and ε. The computational cells can have arbitrary shapes to facilitate the fitting of general curvilinear geometries. With proper boundary conditions set, the system of discretized equations is then solved by an iterative routine with a fast and robust convergence rate.

5.7. The RNG k–ε model

The renormalization group (RNG) k–ε model is similar in form to the standard k–ε model but includes an additional terms for dissipation rate ε that significantly improve the accuracy, especially for rapidly strained flows. The effect of swirl on turbulence is included in the RNG model, enhancing accuracy for swirling flows. The RNG k–ε model has a similar form to the standard k–ε model:

$$\frac{\partial}{\partial t}(\rho k) + \frac{\partial}{\partial x_i}(\rho k u_i) = \frac{\partial}{\partial x_j}\left(\alpha_k \mu_{\text{eff}} \frac{\partial k}{\partial x_j}\right) + G_k + G_b - \sigma\varepsilon - Y_M + S_k \tag{19}$$

and

$$\frac{\partial}{\partial t}(\rho k) + \frac{\partial}{\partial x_i}(\rho \varepsilon u_i) = \frac{\partial}{\partial x_j}\left(\alpha_\varepsilon \mu_{\text{eff}} \frac{\partial \varepsilon}{\partial x_j}\right) + C_{1\varepsilon}\frac{\varepsilon}{k}(G_k + C_{3\varepsilon}G_b) - C_{2\varepsilon}\rho\frac{\varepsilon^2}{k} - R_\varepsilon + S_E \tag{20}$$

In these equations, G_K represents the generation of turbulence kinetic energy due to the mean velocity gradients. G_b is the generation of turbulence kinetic energy due to buoyancy; Y_M represents the contribution of the fluctuating dilatation in compressible turbulence to the overall dissipation rate; α_k and α_ε are the inverse effective Prandtl numbers for k and e, respectively. S_K and S_E are user-defined source terms.

6. Experimental set up

Experimental set up was established in the departmental lab to study the hydrocyclones. The schematic of the set up is as shown in Fig. 1. The set up consisted of a hydrocyclone, rotameter, centrifugal pumps and storage tanks for inlet supply and overflow–underflow water collection. The material used for constructing the hydrocyclones was transparent Perspex. The photographic view of the hydrocyclone is shown in Fig. 2. The set up of hydrocyclone had a cone mounted by a cylinder. The total height of cone and cylinder was 58.1 cm in which the length of the conical portion was 36.5 cm. The diameter of the cylindrical portion was 10 cm. hydrocyclones have no moving parts, and pumping the fluid tangentially into the stationary conocylindrical body produces the essential whirling motion. The cylindrical part is closed at the top by a cover, through which the liquid overflow pipe, known as the vortex finder, extends 12.5 cm into the cyclone body. Located near the top cover at a distance of 3.1 cm was a circular feed opening where liquid enters the hydrocyclone through the cylindrical tangential inlet of 2.5 I.D. The mercury manometers were provided to measure the pressure drop across the hydrocyclone. A high capacity tank is provided to collect recycled liquid from apex pipe and overflow pipe and to recycle back to inlet section of the hydrocyclone. A small tank is provided at bottom section to collect underflow liquid and recycled to large storage tank. A rod insertion hole was also made to eliminate the air core, which was closed when air core was desired. The formation of air core at 45 LPM is shown in Fig. 3. Centrifugal pump is provided to feed process liquid to hydrocyclone. Rotameter is installed to measure total inlet volumetric flow rate to the hydrocyclone. Respective valves are installed to control the water flow. Mercury manometers measure the pressure at overflow, underflow, inlet and at the middle section of the cone. The detailed dimensions of the system presented in Table 1. The density of the tracers used for separations are mainly type-1 (lighter), type-II, type-III and type-IV (denser) with specific gravity 0.97, 1.03, 1.27 and 1.57, respectively.

Fig. 2. Photograph of the hydrocyclone column.

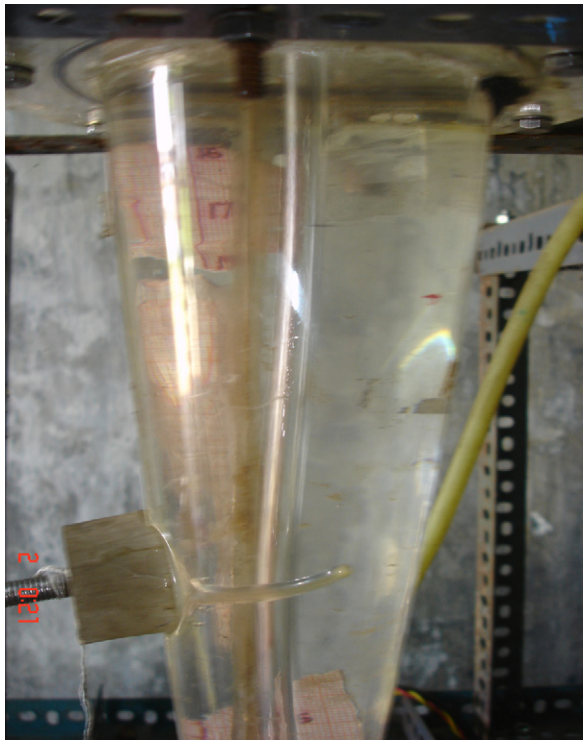

Fig. 3. Formation of air core at 45 LPM.

7. Experimental methodology

In this experiment we studied the effect of air core on the pressure drop of the hydrocyclones between inlet and underflow, inlet and overflow, overflow and underflow, an interior point of the conical portion of the hydrocyclone and overflow. We made a new arrangement for the removal of air core. We inserted a solid rod first horizontally through the conical portion then through the bottom, vertically. In Horizontal insertion a rod of diameter 8 mm was inserted and the length of the rod was varied from 0, 0.5 and 1.0 times the conical diameter in the plane of the hole as shown in Fig. 4. Then a similar kind of experiment was varied with vertical insertion. Then two rods of diameter 6.68 and 4.58 mm were inserted from the bottom of the hydrocyclone, i.e.

Table 1
Dimensions of the hydrocyclone column

Component of the hydrocyclone	Measurements (cm)
Internal diameter of the cylinder	10.0
Length of cylindrical portion	21.6
Length of the conical portion	36.5
Diameter of the underflow pipe	2.5
Diameter of the vortex finder pipe	1.8
Diameter of the feed inlet	2.5
Vortex finder depth	12.5

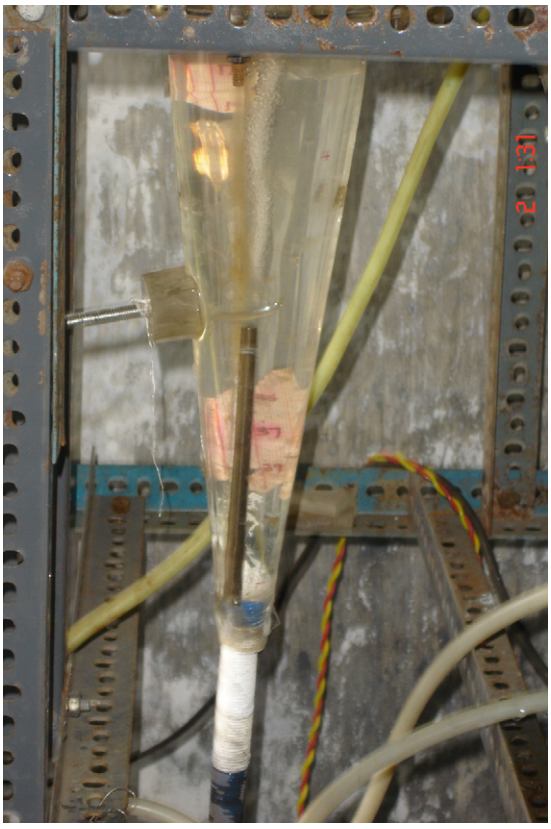

Fig. 4. Vertical insertion of the rod at a distance of 19.6 cm from the apex.

from the underflow outlet. The 6.68 mm diameter rod insertion was done first at an insertion from the 0, 19.5 and 25.5 mm, and pressure drop readings were taken. Similarly, the 4.58 mm diameter rod was inserted at 0, 19.5 and 25.5 mm diameter.

The experimental procedure explained above is repeated three to four times for each condition during experiment to minimize the experimental errors and the arithmetically averaged values were taken as a result.

8. Results and discussion

Experiments have been made for different inlet volumetric flow rate and with air core and without air core to characterize the pressure drop characteristics of hydrocyclones. Experiments were conducted at total inlet volumetric flow rates of 35, 45 and 55 LPM. The various setting that was used was:

1. First the readings with air core were taken and flow rates were varied from 35 LPM, then 45 LPM and then 55 LPM to see the pressure drop with the unhindered formation of air core.
2. Then the horizontal insertion was made which eliminated the air core. The rod was inserted in two phases. Firstly rod was inserted up to half of the cone diameter then the rod was inserted completely to see the effect of varying air core on pressure drop.
3. Then we made vertical insertion of rod through the apex cone to stop the formation of air core. We varied the rod diameter as well as the length of the rod inside the hydrocyclone geometry.

Pressure drop in a hydrocyclone varies with the flow rate as shown in Figs. 5–8. The effect of air core formation on the pressure drop is studied. The pressure drop between inlet and underflow increases with the increase in inlet velocity from low to medium values that again increases when we move from medium to high values as shown in Fig. 5. Similarly, the pressure drop between overflow and the interior point of on the conical part increases with the rise in velocity shown in Fig. 6. This phenomenon can be explained on the basis of formation of air core.

At a particular set of fixed parameters, starting from the condition of flow rate at which air core is formed total inlet flow rate is increased from low to high flow rate. If we increase the total inlet flow rate from low to medium flow rate, the size of air core increases.

Again if the flow rate is increased from medium to high flow rate the size of air of core is increased further and it becomes more stable and forms like a solid core structure inside the hydrocyclone. The thickening of air core brings a lot of turbulence with it into the hydrocyclone, which results in high-pressure drops. The vertical insertion of the rod at a distance of 19.6 cm from apex eliminates the formation of air core.

A horizontal rod of 8 mm was inserted inside the conical portion, which caused the elimination of air core in the vortex. The pressure drop between inlet and the underflow decreases as the rod is inserted into the hydrocyclone from completely outside the cone to 50% inside the conical portion then completely covering the diameter of the conical portion. Pressure drop also increases as the inlet velocity is increased from low values (35 LPM) to moderate values (45 LPM) and then from moderate values to higher values (55 LPM) for inlet and underflow. Overflow and the fixed interior point on the hydrocyclone follow almost similar trend (see the schematic). However, the pressure drop between underflow and overflow follows an opposite trend.

The higher pressure drops for lesser insertion of rod can be explained on the basis of formation air core, which causes more pressure drop because of increasing disturbances. The more pressure drops while increasing the inlet velocity are also in sync with the belief that the pressure drop increases with an increase in flow rate as shown in Fig. 7.

A vertical rod of 6.68 mm was inserted inside the conical portion from the apex, which caused the elimination of air core in the vortex. The pressure drop between inlet and the underflow decreases as the rod is inserted into the hydrocyclone from completely outside the cone to 19.5 cm inside the conical portion then 25.5 cm into the hydrocyclone. Pressure drop also increases as the inlet velocity is increased from low values (35 LPM) to moderate values (45 LPM) and then from moderate values to higher values (55 LPM) for inlet and underflow. Overflow and the fixed interior point on the hydrocyclone follow almost similar trend (see the schematic). However, the pressure drop follows an opposite trend between underflow and overflow. In Fig. 8 the higher pressure drops for lesser insertion of rod can be explained on the basis of formation air core, which causes more pressure drop

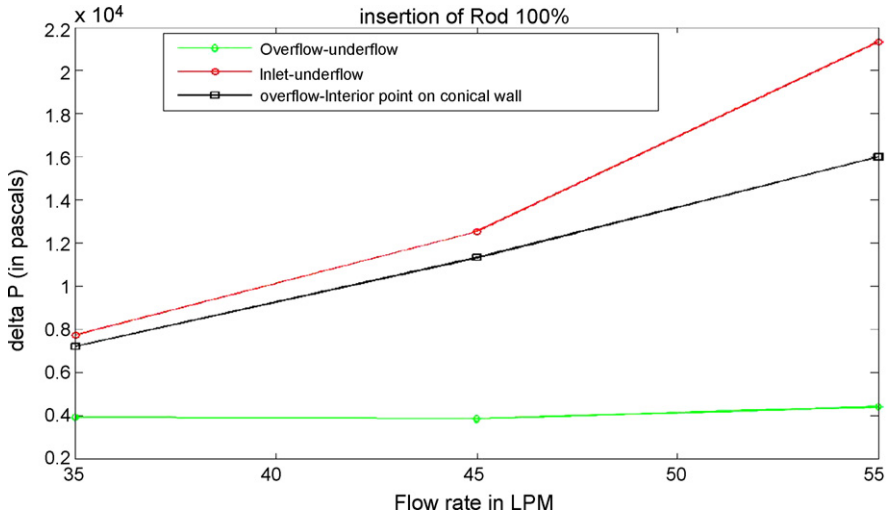

Fig. 5. Effect of water flow rate on pressure drop ΔP (in Pascal) between various points on the hydrocyclones for complete insertion of the rod in horizontal plane of conical orifice.

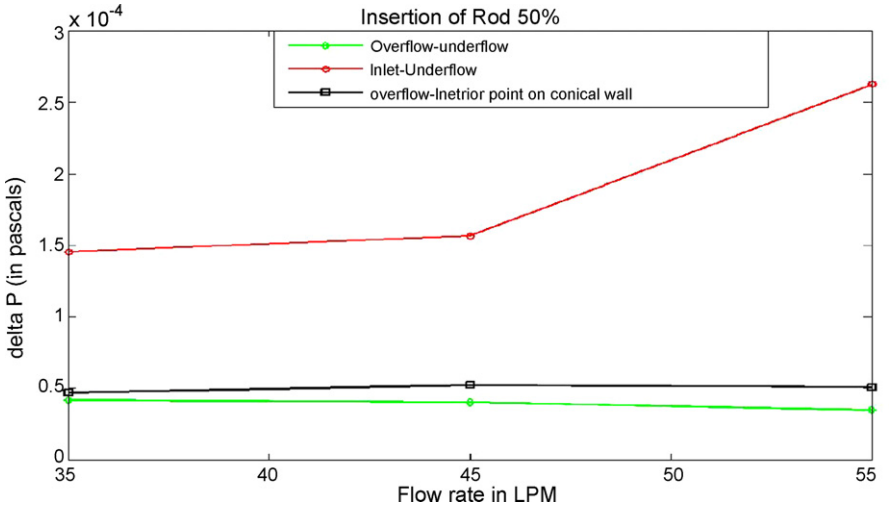

Fig. 6. Effect of water flow rate on pressure drop ΔP (in Pascal) between various points on the hydrocyclones for 50% insertion of the rod in horizontal plane of conical orifice.

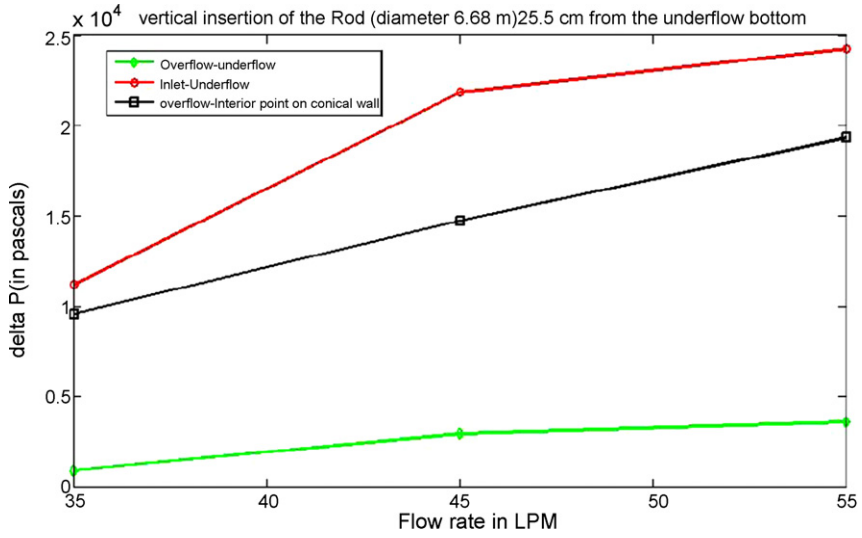

Fig. 7. Variation of ΔP (Pascal) between various points on the hydrocyclones with the change in flow rate (when a vertical rod of diameter 6.68 mm is inserted through the underflow opening to a depth of 25.5 cm).

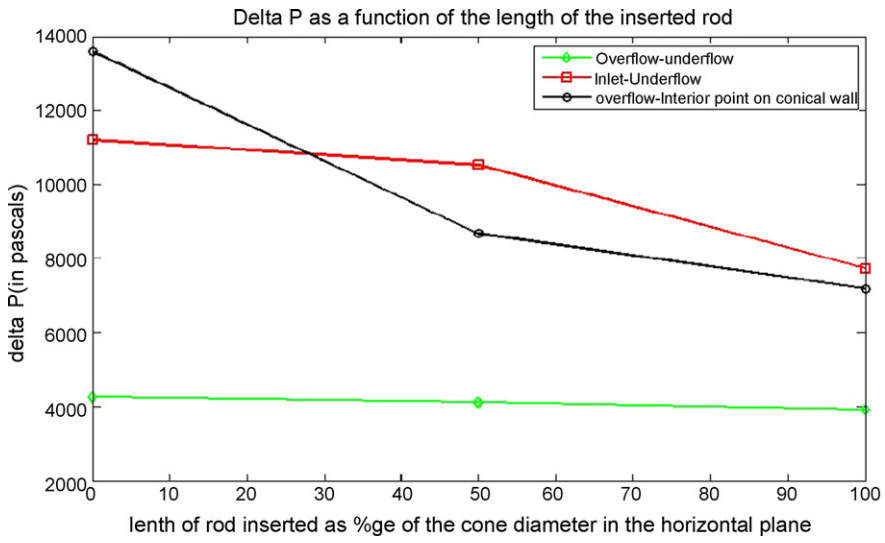

Fig. 8. Variation of ΔP (Pascal) with the length of the inserted rod as %age of the cone diameter in the horizontal plane (inlet flow = 35 LPM).

because of increasing disturbances. The more pressure drops while increasing the inlet velocity are also in sync with the belief that the pressure drop increases with an increase in flow rate.

The trends are almost similar for the vertical and horizontal insertion. However, the vibrations are very high when we put inside a vertical rod and a lot of external power has to be applied to hold the tube stationary.

8.1. Modelling and simulation

8.1.1. FLUENT: an introduction

FLUENT is the worlds' largest provider of commercial computational fluid dynamics software and services. FLUENT offers general-purpose CFD software for a wide range of industrial applications, along with highly automated, specifically focused packages.

FLUENT is a state-of-the-art computer program for modelling fluid flow and heat transfer in complex geometries. FLUENT provides complete mesh flexibility, including the ability to solve flow problems using unstructured meshes that can be generated about complex geometries with relative ease. The different stages are presented in Fig. 9(a).

CFD simulations generally are done in three basic steps

- pre-processing,
- solving and
- post processing.

8.1.2. Pre-processing

It consists of the input to a flow problem to a CFD program by means of an operator friendly interface and the subsequent transformation of this input into a form suitable for use by the solver. The user activities at the pre-processing stage involve definition of the geometry of the region of interest, grid generation and setting up the boundary types. This is the first step in building and analysing a flow model. It includes building the model within a computer-aided design (CAD) package such as GAMBIT, T-Grid etc. and creating and applying a suitable computational mesh, and entering the flow boundary conditions and fluid materials properties. Among a wide range of geometry tools, Boolean operators provide a simple way of getting from a CAD solid to a fluid domain.

8.1.3. Solving

This step involves actually solving the differential equations in the cell domains to get the flow variables and the properties in the control volumes that are defined in the pre-processing step. The scheme selection, boundary conditions, initialization and setting the residuals also come within this step before solving the equations. The FLUENT CFD code has extensive interactivity, so we can make changes to the analysis at any time during the process. This saves you time and enables you to refine your designs more efficiently. Graphical user interface (GUI) is intuitive, which helps to shorten the learning curve and makes the modelling process faster.

8.1.4. Post processing

This step contains showing the results that are obtained by the solver in terms of graphs and plots. Drawing the vector plots, path lines, streak lines, streamlines and particle tracking comes under this. The output of the post processing gives the representation of the flow.

8.2. Generation of geometry

GAMBIT is acronym for Geometry and Model Building Intelligent Toolbox. It is an application software that helps creating complex geometries and meshing them easily. It offers wide range of meshing styles and strictly follows the rules of solid geometry that makes it easy to form desired geometries. It also helps user to automatically select meshing schemes that are appropriate for the geometry being worked on. The geometry in GAMBIT used is shown in Fig. 9(b).

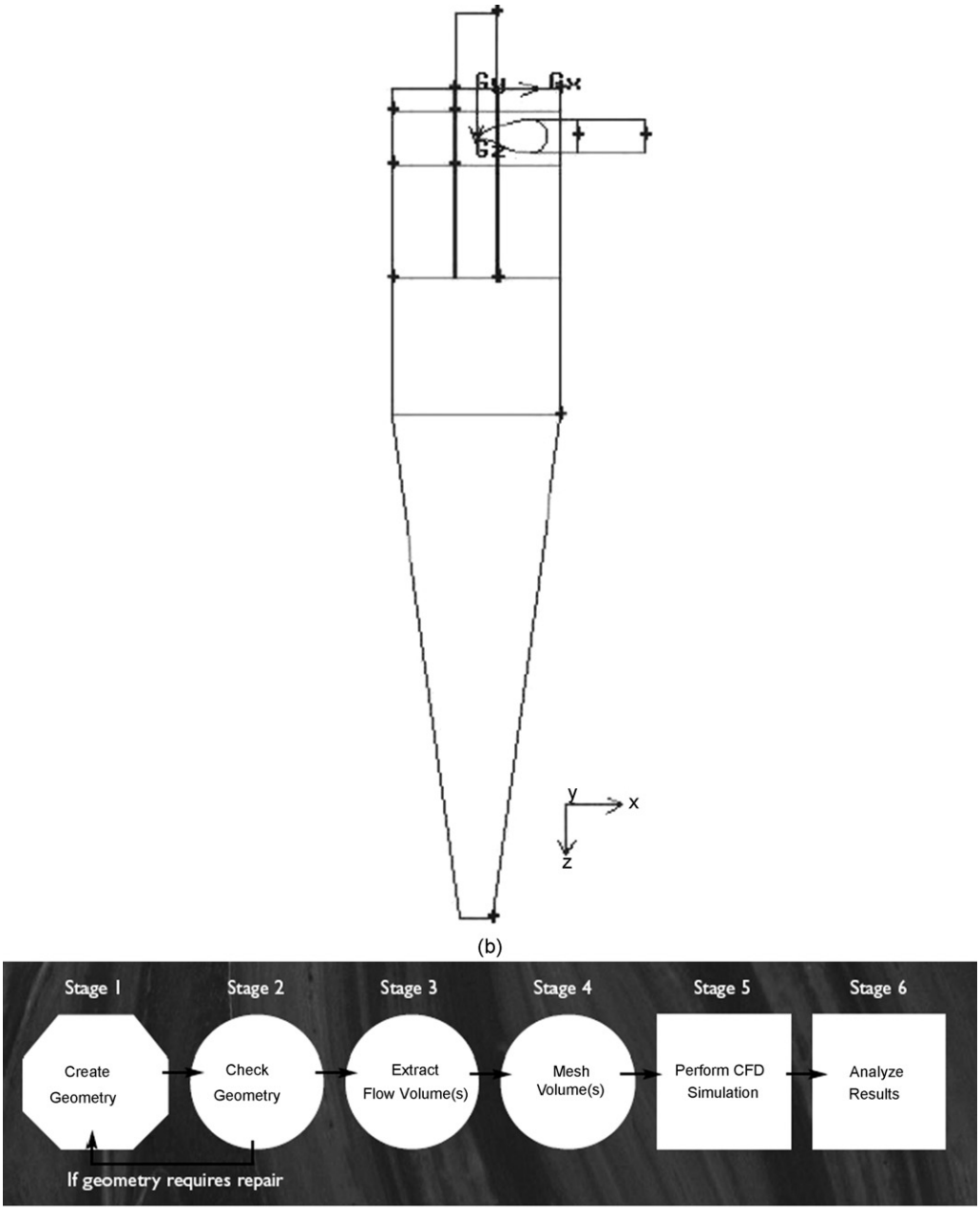

Fig. 9. (a) Stages of analysis and (b) geometry in GAMBIT.

8.3. Pre-processing: building geometry in GAMBIT

The geometry was built in GAMBIT. The steps followed to make such a geometry that consists of two geometries (cylinder and a cone) joined with each other and having different types and sizes of grids as follows:

8.3.1. Meshing

The following features were added for the simulation of proposed model

1. The mesh used has to be an unstructured Hex mesh for the main body of the cyclone. In strongly convective flows, as in a cyclone, it is best to align the mesh to the flow direction this prevents false diffusion.
2. Hexahedral mesh elements are less diffusive than other mesh element shapes such as tetrahedral. In addition to the Hex elements it is preferential to use high order discretization to further reduce the influence of false or numerical diffusion. In this example the tangential inlet shown is meshed for simplicity using tetrahedral elements. The tangential inlet is also joined to the main cyclone chamber by a small overlapping non-conformal interface.
3. A non-conformal interface interpolates the fluxes from one part of the mesh to the other and is an easy method of joining two different mesh types. Although the geometry presented in the papers is relatively straightforward this methodology means more complicated examples of inlet are easy to manipulate and eases the automation process. Tetrahedral mesh

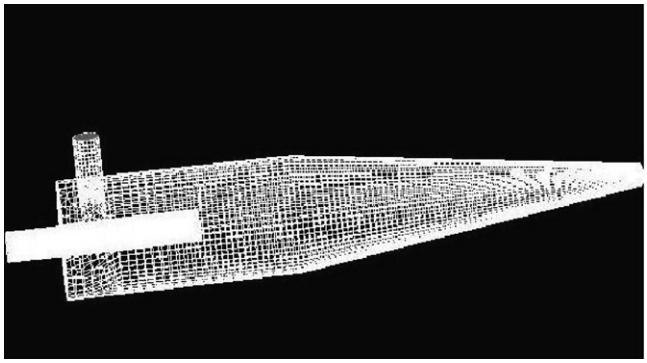

Fig. 10. Meshed geometry.

elements easily accommodate acute geometry in particular the point where the inlet joins the cylindrical cyclone.

4. The non-conformal interface means that pre-generated libraries of inlet can be built and easily connected to the model within the template. Non-conformal interfaces are susceptible to interpolation error, to minimize this, the mesh size needs to be comparable.
5. A boundary layer mesh has to be used near the wall of the cyclone. Although boundary layer resolution is not critical when modelling cyclones as the turbulence is generated in the main flow. At the underflow a narrow annular gap may form due to the air core this needs to be well resolved.

The meshed geometry is shown in Fig. 10. Due to radial pressure gradients in the cyclone because of the high swirl a radial pressure distribution has to be applied to the under and overflow. A velocity inlet is used to prescribe the flow of slurry into the cyclone. When using a RNG model it is necessary to run the simulation for a significant number of iterations, beyond normal convergence criteria. The overflow and underflow were defined as pressure outlets and the inlet as velocity inlet. Rest of the body surface was considered as wall. The geometry with mesh was then exported to Mesh file for FLUENT 5/6 solver. The extended grid and meshed grid front view shown in Figs. 11 and 12. Above completes the pre-processing part of FLUENT Simulation problem. Now this geometry was used in FLUENT Software for simulation.

8.4. Problem solving in FLUENT

Stepwise explanation of important steps in simulation of the problem follows:

- FLUENT was started in 3D mode.
- The Mesh file was imported. The grid was checked for limit sizes. The grid was then scaled to cm scale and smoothened and swapped.
- Implicit, steady and segregated solver was selected.
- RNG k–ε model was used for the simulation.
- Two phase flow of air and water was considered.
- Simulations were done for three sets of inlet velocities, i.e. 1.58, 1.96, 2.2 m/s.

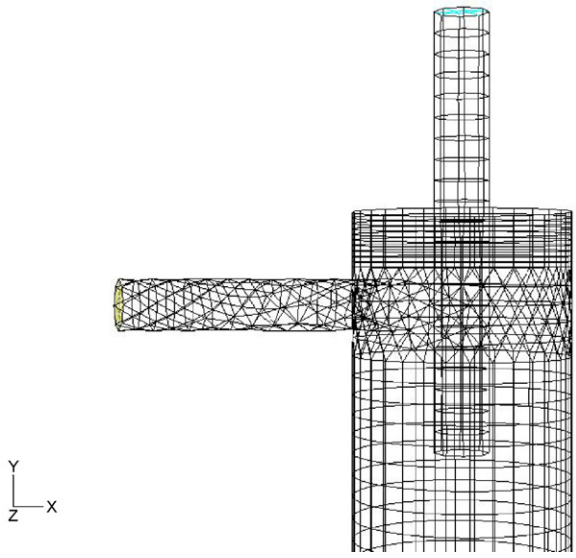

Fig. 11. Extended grid.

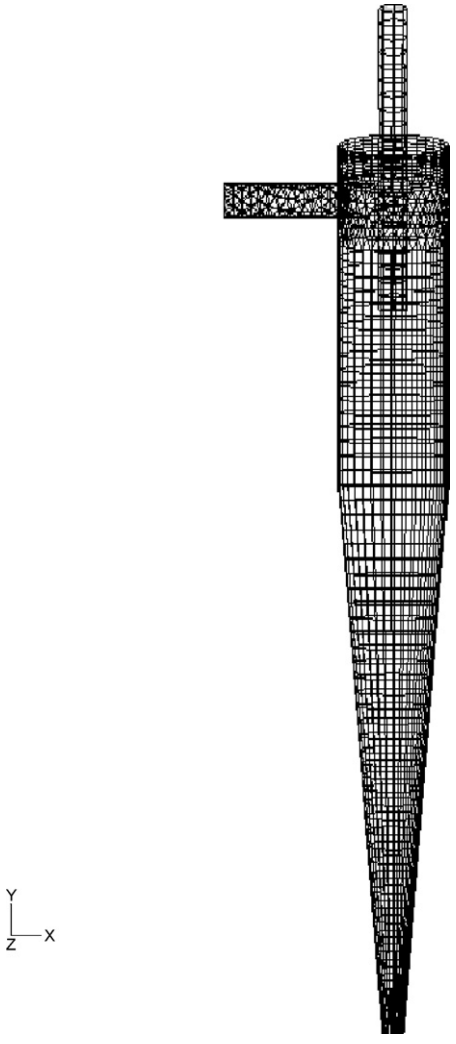

Fig. 12. Meshed grid—front view.

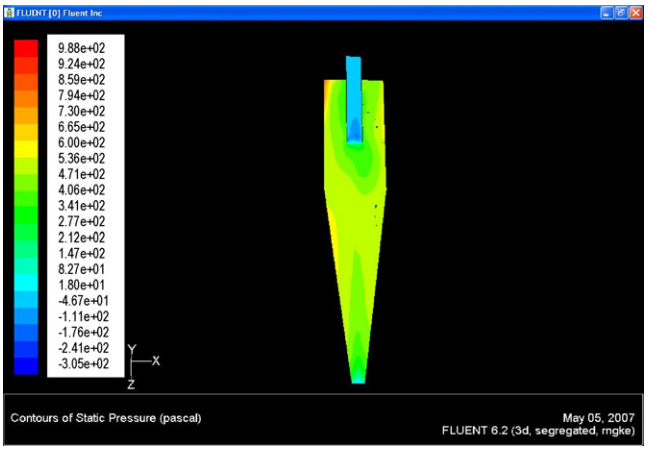

Fig. 13. Static pressure contour.

- Water as a material was imported from FLUENT database and boundaries and continuums were defined.
- The gauge pressure at top surface was set to zero and gravity effect was introduced in operating conditions.
- SIMPLE algorithm for pressure–velocity coupling was used in solution control and at the same time, standard discretization of pressure and power law discretization of momentum were assigned. Under relaxation factors were also set.
- The system was initialised; residual monitoring was set (10^{-3} for each of continuity equation, and three velocity equations).
- Iterations were started with fixed time steps of 0.01 s and desired number of iterations.

9. Results and discussion

The contour of pressure and velocities were studied for three different velocities for which the results are as follows:

Fig. 13 shows that the pressure drops radially as we move from outer to inner parts of the hydrocyclone. This also explains the reason for formation of lower pressure region, which results in the formation of air core. In Fig. 14 as we move radially inward the decreasing tangential velocity is observed which again increases after a while. The underflow is denoted by the

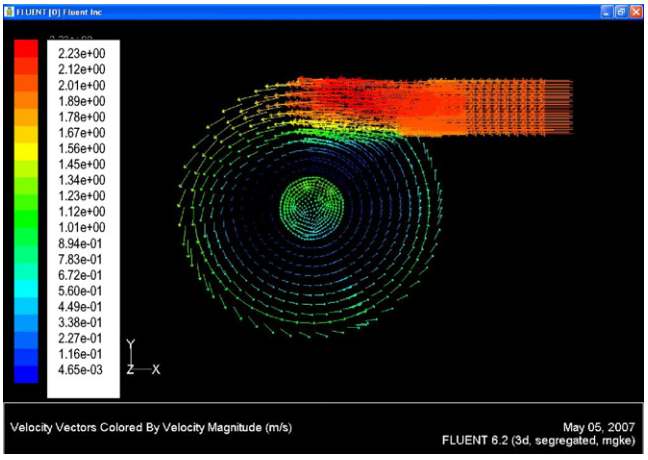

Fig. 14. Velocity profile (near inlet).

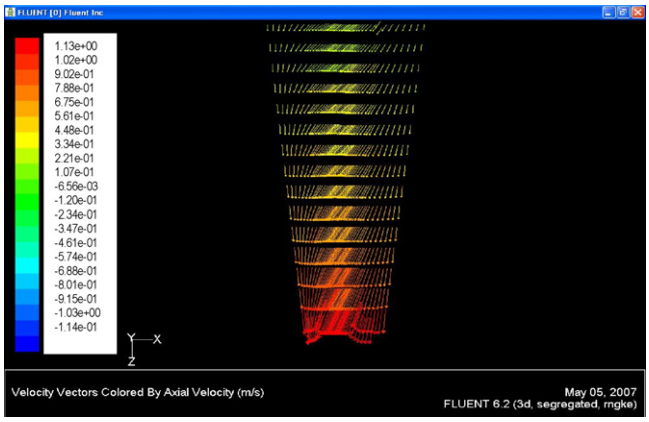

Fig. 15. Axial velocity profile near underflow.

downward pointing velocity vectors in Fig. 15. At the middle of the cone the reversal of velocity vector is observed, which expands as we go up toward the top of the hydrocyclone. The magnitude of the velocity drops moving radially inward to the cyclone but again increases as we go further. This clearly indicates the formations of two vortexes with opposite directions of vertical velocity. This may be because of mass balance in the hydrocyclone. The inlet flow rate is greater than the apex flow rate which in turn allowed the rest of fluid to flow through the vertex. Fig. 15 clearly shows in the middle of the cone the reversal of velocity vectors, which expands as we go up toward the top of the hydrocyclone. The changing directions of the velocity vectors and change in the magnitudes of the velocity are shown in Fig. 16, which shows the velocity profiles near the hydrocyclone overflow. Fig. 16 gives a very clear picture of velocity profile near the vortex finder. The velocity becomes almost axial and the radial and tangential components become minimal. Thus separations of particles reported in the overflow more. Fig. 17 presents the velocity profile at three different heights. The upper small dense bright circle shows velocity vectors of almost same order, i.e. this is the underflow region. The lower larger circle has two scattered region; the inner one shows the minimum flow velocity through vortex finder and the outer one is the surrounding of vortex finder. The middle circle shows a region anywhere between underflow and overflow.

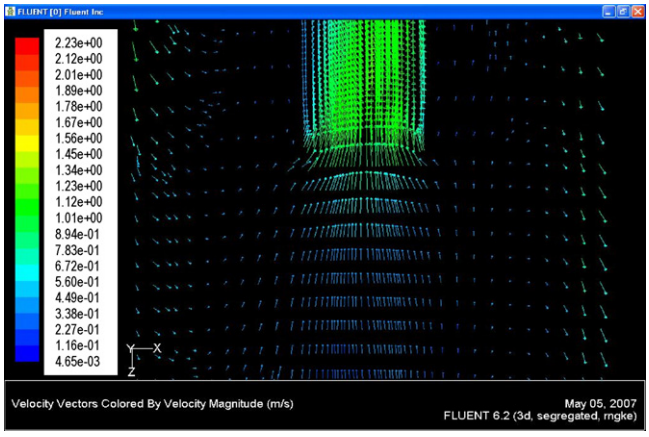

Fig. 16. Velocity vector near overflow.

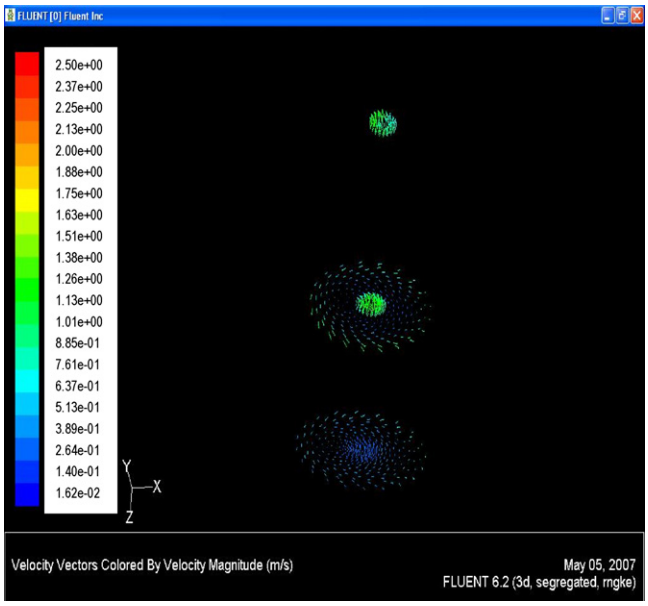

Fig. 17. Velocity vectors at different heights.

The figures show that the flow is under high centrifugal and turbulent actions. The two vortexes at different heights are also observed.

10. Conclusions

The main purpose of this experiment was to study the pressure drop across the hydrocyclone geometry. The effect of air core formation on the pressure drop and again the variation of pressure drop with the flow rates were studied. The effect of air core on pressure drop can be explained as the air core causes more turbulence inside the hydrocyclone and thus there is more pressure drop because of more swirls. We can see that as the flow rates increase the air core which was almost like a small wave gets thicker and thicker increasing the disturbance inside the hydrocyclone which leads to higher pressure drop. There are two kinds of vortex, which are formed inside a hydrocyclone. They are opposite in the direction of vertical velocity. One causes the lighter particles to go out from the top and other causes heavier particles from the bottom. The velocity magnitude is more at the inlet section of the hydrocyclone, medium at overflow and underflow section and minimum at middle sections of the hydrocyclone. It is observed that low-pressure zone is created at the central axis of the hydrocyclone. When both top and bottom sections are open to the atmosphere, air is sucked inside the hydrocyclone body and air core is formed which has the same pressure as that of the atmospheric pressure. The flow is under highly turbulent and centrifugal action inside the hydrocyclone. The velocity magnitude at the underflow and interiors of the hydrocyclone are under the action of centrifugal force and which is observed from the direction of the velocity vectors at the underflow section. The radial velocity is negligible at the inlet section of the hydrocyclone. Minimum values of radial velocities are observed at the whole body of the hydrocyclone but maximum values are at the apex and overflow section.

Acknowledgement

Authors thankfully acknowledge M/S Tata Steel, Jamshedpur for the financial grant sanction to Department of Chemical Engineering, IIT Khargpur, India to carry out part of the research work.

References

[1] E. Bretney, Water Purifier, U.S. Patent No. 453, 105A 1891.
[2] D.F. Kelsall, A study of the motion of solid particles in a hydraulic cyclone, Trans. Inst. Chem. Eng. 30 (1952) 87–107.
[3] D. Bradley, D.J. Pulling, Flow patterns in the hydraulic cyclone and their interpretation in terms of performance, Trans. Inst. Chem. Eng. 37 (1959) 34–45.
[4] A.J. Lynch, T.C. Rao, Studies on the operating characteristics of hydrocyclone classifiers, I. J. Tech. 6 (1966) 106–114.
[5] L. Chu, W. Chen, X. Lee, Enhancement of hydrocyclone performance by controlling the inside turbulence structure, Chem. Eng. Sci. 57 (2002) 207–212.
[6] K.T. Hsieh, R.K. Rajamani, Mathematical model of the hydrocyclone based on physics of fluid flow, AIChE J. 37 (5) (1991) 735–746.
[7] P.R. Steffens, W.J. Whiten, S. Appleby, J. Hitchins, Prediction of air core diameters for hydrocyclones, Int. J. Min. Process. 39 (1993) 61–74.
[8] T. Dyakowski, R.A. Williams, Modelling turbulent flow within a small-diameter hydrocyclone, Chem. Eng. Sci. 48 (6) (1993) 1143–1152.
[9] S.D. Laverack, The effect of particle concentration on the boundary layer flow in a hydrocyclone, Trans. Inst. Chem. Eng. 58 (1980) 33–42.
[10] R.K. Dwari, M.N. Biswas, B.C. Meikap, Performance characteristics for particles of sand FCC and fly ash in a novel hydrocyclone, Chem. Eng. Sci. 59 (2004) 671–684.
[11] E. Ovalle, F. Concha, The role of wave propagation in hydrocyclone operations II: wave propagation in the air-water interface of a conical hydrocyclone, Chem. Eng. J. 111 (2005) 213–223.
[12] M.R. Davidson, Similarity solutions for flow in hydrocyclones, Chem. Eng. Sci. 43 (7) (1988) 1499–1505.
[13] P. He, M. Salcudean, I.S. Gartshore, A numerical simulation of hydrocyclones, Trans. Inst. Chem. Eng. Part A 7 (1999) 429–441.
[14] G.Q. Dai, J.M. Li, W.M. Chen, Numerical prediction of the liquid flow within a hydrocyclone, Chem. Eng. J. 74 (1999) 217–223.
[15] K. Rietima, Performance design of hydrocyclones, Chem. Eng. Sci. 15 (1961) 298–325.
[16] M. Frachon, J.J. Cilliers, A general model for hydrocyclone partition curves, Chem. Eng. J. 73 (1999) 53–59.
[17] R. Clift, J.R. Grace, M.E. Weber, Bubbles, Drops and Particles, Academic Press, New York, 1978.